CONF-75-104-E
E-0026

MSU-CSL-25
July, 1975

DEEP INELASTIC MUON SCATTERING AT FERMILAB†*

K. Wendell Chen
Michigan State University, East Lansing, Michigan 48823

Invited Talk
International Conference on High Energy Physics
Palermo, Italy
July 23-27, 1975

†Supported by the National Science Foundation.

*Operated by Universities Research Association Inc. under contract with the Energy Research and Development Administration

1. INTRODUCTION

Since 1973 a program to study the validity of scale-invariance in high energy muon scattering has been underway at Fermi National Accelerator Laboratory, Batavia, Illinois. The experimental results of this investigation are presented at this conference. We find significant deviations from scale-invariance in:

i) ratios of muon scattering cross sections at 150 and 56 GeV.[1] (Method I)

ii) comparison of muon scattering data at 150 and 56 GeV with a fit to low energy ep data.[2] (Method II)

2. SCALE-INVARIANCE IN DEEP INELASTIC PHENOMENA

2.1 Cross Sections

The strikingly simple character of deep-inelastic electron scattering led to scaling models of the structure of the nucleon as a composite of structureless entities. Cross sections for deep inelastic scattering can be written as:

$$\frac{d^2\sigma}{dQ^2 d\nu} = \frac{4\pi\alpha^2}{Q^2}\frac{E'}{E_o}\left[W_2\cos^2\frac{\theta}{2} + 2W_1\sin^2\frac{\theta}{2}\right] \tag{1}$$

$$\simeq \frac{4\pi\alpha^2}{Q^2}\frac{1}{\nu}\frac{E'}{E_o}\left[1+\frac{1}{1+R}\left(\frac{E_o}{E'}+\frac{E'}{E_o}-2\right)\right]\nu W_2 \tag{2}$$

where $\nu = E_o - E'$, $x = Q^2/2m\nu$, $y = \nu/E_o$, and $R = \sigma_s/\sigma_t$. For small scattering angles the cross section can be written as:

$$\frac{d^2\sigma}{dxdy} = \frac{4\pi\alpha^2}{2mE_o}\frac{\nu W_2(x,Q^2)}{x^2y^2}\left[1-y+y^2/2(1+R)\right]. \tag{3}$$

Existence of structureless entities implies that the structure function νW_2 must be a function of a single scaling variable,[3] say $\omega = 2m\nu/Q^2$. The experimental evidence for "scaling" was presented initially by SLAC in 1968 in Vienna.[4] The $\theta = 6°$ data as presented by the SLAC-MIT collaboration indicated a scaling behavior predicted by Bjorken. Subsequent measurement reinforced this picture.[5]

2.2 Summary of SLAC-MIT data[6]

A brief summary of the SLAC-MIT data ($E_o \leq 20$ GeV) showing the scaling characteristics are as follows:

*C. Chang, K. W. Chen, D. J. Fox, L. N. Hand, S. H. Herb, A. Kotlewski, P. F. Kunz, S. C. Loken, A. R. Russell, M. Strovink, and W. Vernon.

i. $\sigma_T \simeq \frac{1}{Q^2} f(\omega)$ for $Q^2 \geq 1{\cdot}2\ (\mathrm{GeV}/c)^2$, $\omega = \frac{2m\nu}{Q^2}$

This statement was modified by Bloom and Gilman[7] to

$$\sigma_T \simeq \frac{1}{Q^2} f(\omega') \text{ where } \omega' = \omega + \frac{m^2}{Q^2} \cong \frac{W^2}{Q^2} .$$

ii. $R = \frac{\sigma_S}{\sigma_T} \simeq 0.18$

iii. $f(\omega') \simeq (\omega'-1)^3$ for $\omega' \leq 2$

iv. $f(\omega') \simeq$ constant $\omega' > 4$

v. $\sigma_{en}/\sigma_{ep} \simeq \begin{matrix} 0.3 & \omega' \sim 1.2 \\ 0.85 & \omega' \sim 20 \end{matrix}$

vi. $\lim_{Q^2 \to 0} \sigma_T(Q^2, W^2) = \sigma_\gamma(W^2)$

As a result of these experimental efforts a well-investigated theoretical picture has emerged to interpret the data and to present additional predictions as well as speculations. Much has been written about the quark-parton model, light cone properties of products of currents, duality, generalized vector-meson dominance, as well as numerous other theoretical attempts. On the other hand, after the evidence for scale-invariance first appeared, field-theoretic description of behavior of products of hadron currents at short distances have also predicted specific form of scaling breakdown.

2.3 Ambiquities in tests of scale-invariance

In tests of scale-invariance, the high precision of deep inelastic ep data obtained at SLAC accelerator has been offset by the inability to resolve an ambiquity parameterizing the approach to the scaling region at low ω ($= 1/x \to 1$) and by kinematic bounds on Q^2 and sufficiently high $\omega(\omega > 10)[Q^2 \cdot \omega \leq 29.1]$. Significant deviations from scaling were made to vanish if, instead of the Bjorken scaling variable ω, the variable $\omega' \simeq \omega + m^2/Q^2$ was used instead.[7] Tests of scaling at higher energy (and Q^2) are needed to avoid ambiquity due to non-leading terms and thereby further probe the structure of nucleons at smaller distances.

A high energy muon beam ($E_\mu = 150$ GeV) recently became available at the Fermi National Accelerator Laboratory. As a result, muon scattering data are available at higher ν and Q^2, which can be interpreted more directly with greater certainty. (Figure 1).

3. DEEP INELASTIC MUON SCATTERING AT 150 GeV and 56 GeV

3.1 Preliminary data presented at London and PRL, 1974

The apparatus and NAL muon beam are shown in Fig. 2 and Fig. 3. Early results at 150 GeV presented in London and published recently[8] already show some indications of scaling breakdown. (Figure 4). The preliminary data consist of approximately ≤ 30% of the data. An examination of Fig. 4 shows that there is a sizable systematic trend of the data vs Q^2. At $\langle Q^2 \rangle = 8\ (\mathrm{GeV}/c)^2$ ($\langle \omega \rangle \approx 20$) a + 20% "rise"[Fig. 4(b)] is visible. As $\langle Q^2 \rangle$ increases to $44\ (\mathrm{GeV}/c)^2$ ($\langle \omega \rangle \approx 2$), the data show a systematic depletion to -20%. Although the indication of scale-breaking is observed, the evidence presented was not overwhelmingly conclusive.

At this conference more data collected at 150 GeV and 56 GeV are presented. Final analyses of the results are given below. Two tests were made. Results from both tests are consistent with each other.

3.2 Test I: measurement of scale-invariant ratios of muon scattering cross sections at 150 and 56 GeV.

3.2.1 Measurement of the ratio

The apparatus was constructed to measure the direct ratio of scale-invariant differential cross sections at 150 and 56 GeV. Let the experimentally measured ratio, $\underline{r}(\omega, Q^2)$, be defined by

$$\underline{r}(\omega, Q^2) = \frac{E \frac{d^2\sigma}{dxdy}(E=150)}{E \frac{d^2\sigma}{dxdy}(E=56)} . \tag{4}$$

The experimental apparatus was scaled to change experimental quantities by $\lambda = 8/3$, (Fig. 2).

$E_o \rightarrow \lambda E_o$ (increase muon energy from 56 GeV to 150 GeV)

$E' \rightarrow \lambda E'$ (increase total field integral by 8/3)

$\theta \rightarrow \frac{1}{\sqrt{\lambda}}\theta$ (move target to spectrometer distance by $\frac{1}{\sqrt{\lambda}}$)

As a direct result of these transformations, $\nu \rightarrow \lambda\nu$ and $Q^2 \rightarrow \lambda Q^2$, so that ω remains unchanged.

Scattered muons corresponding to scaled values of ν and Q^2 pass through identical positions in the spectrometer aperture, thereby minimizing possible systematic uncertainties. If Bjorken scaling were to hold in the high energy ($E >> 20$ GeV) region, the ratio should be unity at all values of ω and Q^2, independent of the average value of $\underline{r}(Q^2, \omega)$. Since $d^2\sigma/dxdy \rightarrow 1/\lambda\ (d^2\sigma/dxdy)$ we have,

$$\underline{r}(Q^2, \omega) = \text{constant} \tag{5}$$

for <u>all</u> values of ω and Q^2.

In this test of scaling, the target thickness is also scaled, 622 gm/cm^2 at 150 GeV and 233 g/cm^2 at 56 GeV to give equal count rates per unit incident muon.

At 150 GeV the apparatus was operated at two geometries to accept scattered muon angles, θ, over the full azimuth in the ranges $0.11 \leq \theta \leq 0.48$ (SA) and $0.017 \leq \theta \leq 0.065$ (LA). For the two corresponding 56-GeV configurations the apparatus was scaled to preserve the acceptance and resolution.

Experimental details and internal consistency checks are presented in two submitted papers to the conference. The measurement of the ratio $\underline{r}$ was corrected for experimental nonscaling effects which are in decreasing order of importance: i) differing radial distribution of the muon beam, ii) inexact scaling of spectrometer resolution and acceptance, and iii) radiative corrections. Combined corrections for i), ii), and iii) are less than 10%.

3.2.2 Results on measurement of $\underline{r}(Q^2, \omega)$ (Method I)

Figures 5 and 6 depict $\underline{r}$ as a function of only Q^2 or ω. Data in these figures are presented both in combined form and (respectively) in bins of ω and (scaled) Q^2. The hypothesis that any scale-noninvariance is a function only of Q^2 is shown in Fig. 5 by drawing a power-law fit to combined data through data in four $\langle\omega\rangle$ bands. This hypothesis has 16% confidence for either a power-law or a propagator fit in Q^2 (Table 1). The latter is a poor representation of the data since its value at $Q^2 = 0$ exceeds unity.

A statistically more favorable hypothesis is that $\underline{r}$ depends only on ω. In this case the scale-breaking parameter $\underline{b} = \partial^2 \ln(\nu W_2)/\partial \ln(\omega') \partial \ln Q^2$ is nearly equal to the exponent of the power-law fit to $\underline{r}$ vs ω [Table 1(b)]. If assumed to be ω-independent, the parameter $\underline{b}$ is 0.098±0.028. It should be emphasized that $\underline{b}$ is presented only as a guide to the systematic trend of the data. It is not necessarily a physically significant parameter in deep inelastic phenomena.

The dependence of $\underline{r}$ upon systematic effects is also indicated in Fig. 5 and 6. If scaling in ω rather than ω' is tested, $\underline{b}$ shifts upward by 0.047. An increase of 0.057 results from suspending Monte-Carlo corrections, which affect only the end bins in the ω distribution. (Dropping these end bins raises $\underline{b}$ by 0.025.) The effect of using a scale-noninvariant form of R which fits SLAC data is negligible.[10] The ±1% systematic error in relative energy calibration creates an uncertainty of ±0.056 in $\underline{b}$. It is of considerable interest to fit $\underline{r}(Q^2, \omega)$ to a constant in bins of E' and θ with widths smaller than the experimental resolution. The overall average yields 1.02±0.02 indicating that the excess at large ω tends to cancel the depletion at low ω.

3.2.3 Discussion of measurement of $\underline{r}(Q^2, \omega)$ (Method I)

The observed scaling-breaking effects in $\underline{r}(Q^2, \omega)$ show an increase in value at large ω and a corresponding decrease in value at low ω. The form is incompatible with a form-factor type of scaling violation.[9]

If $\underline{r}(Q^2, \omega)$ is assumed to be a function of ω only, i.e.,

$$\frac{\nu W_2(Q^2, \omega)}{\nu W_2(\frac{3}{8}Q^2, \omega)} \text{ is independent of } Q^2,$$

then νW_2 should have a form:

$$\nu W_2(Q^2, \omega) = F(\omega)(Q^2)^{\delta(\omega)}. \tag{6}$$

If $\delta(\omega)$ can further be fit to a $\ln(\omega/\omega_o)$ form, one obtains a value for $\underline{b} = \partial^2 \ln \nu W_2 / \partial \ln \omega' \partial \ln Q^2$:

$$\underline{b} = 0.098 \pm 0.028, \tag{7}$$

and

$$\omega_o = 6^{+9}_{-4}.$$

TABLE 1

Fits to $\underline{r}(Q^2, \omega)$

Fig. Ref.	r =	Confidence Level %	Fitted Parameters	
5	$(v/v_o)^n$	16 (16[a])	$n=-0.083\pm0.032$	$v_o=0.041\pm0.011$
	$\frac{N(1+Q_2^2\Lambda^{-2})^{2^b}}{(1+Q_1^2\Lambda^{-2})^2}$	9 (16[a])	$\Lambda^{-2}=(50^{+29}_{-26})\times 10^{-4}$	$N=1.079\pm0.035$
6	$(\omega/\omega_o)^n$	94 (71[c])	$n=0.096\pm0.028$	$\omega_o=6.08^{+8.86}_{-3.61}$

a) Fit is made to data at all ω. This confidence level applies to the same best fit compared to data broken into 4 bands of ω (Fig. 5).
b) Q_1^2 (Q_2^2) refers to Q^2 at 150 (56) GeV. This "propagator" fit is constrained to N=1.0 with a gaussian error of ±0.07. The best fit Λ^{-2} corresponds to $\Lambda > 10.7$ GeV (90% confidence).
c) Fit is made to data at all v. This confidence level applies to the same best fit compared to data broken into 3 bands of v (Fig. 6).

3.3 TEST II: Comparison of muon scattering data at 150 and 56 GeV with electron data at 20 GeV

3.3.1 Comparison of μp data (150, 56) with ep (20) data

The second test of scaling compares these cross sections with lower-energy electron-scattering values assuming the validity of μ-e universality. Within fixed bands of ω, variations of νW_2 are evaluated over the full Q^2-range of the data. Thereby, with an accurate Monte-Carlo calculation of the experiment, a scaling test more precise than method discussed in Section 3.2 is possible.

A number of tests establish the accuracy of the Monte-Carlo. Shapes of real and simulated distributions in azimuth and radius of tracks near fiducial boundaries agree

well. The Monte-Carlo accounts for tails in distributions of χ^2 and reconstructed energy through 2.5 decades in population. Also, it accurately models differences between momentum reconstruction algorithms which use different points on the muon trajectories. We believe that inaccuracies in calculating the acceptance and resolution contribute negligible to the overall error.

3.3.2 Results of the comparison

Ratios of observed to Monte-Carlo event rates are shown in Fig. 7 vs $\ln Q^2$ for 8 overlapping bands of ω. Results of straight-line fits to these data points, along with the widths of the ω bands, are given in Table 2. The points show also a rising trend with Q^2 at high ω, and a falling trend at low ω. Fitting a power-law Q^2-dependence in each ω band yields an overall χ^2 of 45.6 for 51 degrees of freedom. Scale-invariance in ω' requires each set of points to exhibit no Q^2-dependence. This hypothesis raises the χ^2 by 36.6 with the addition of 8 degrees of freedom. Statistically, such a fluctuation has a probability smaller than 2×10^{-5}. These 8 fitted slopes $\partial \ln \nu W_2 (\omega', Q^2)/\partial \ln Q^2$ are plotted vs ω in Fig. 8. In the range of these data, the scale-breaking may be parameterized by a quantity $\underline{b} = \partial^2 \ln (\nu W_2)/\partial \ln (\omega') \partial \ln (Q^2)$. If independent of both Q^2 and ω, $\underline{b}$ has the magnitude (when fitted to $\ln \omega/\omega_o$),

$$\underline{b} = 0.099 \pm 0.018$$
$$\omega_o = 6.1^{+3.9}_{-2.4} \; . \qquad (8)$$

Note that the slope $\partial \ln \nu W_2 (\omega', Q^2)/\partial \ln Q^2$ crosses over zero at $\omega' \approx 4$-6 (apparent scaling).

TABLE 2

$\ln$(data/MC) fit to $c + b \ln(Q^2/3)$

$\langle\omega\rangle$ [a]	$\frac{\delta(\omega)}{\omega}$ [a]	c	b	% confidence
3.5	0.60	0.04±0.07	-0.076±0.031	54
3.8	0.53	0.07±0.07	-0.064±0.028	80
4.7	0.52	0.12±0.04	-0.017±0.033	73
5.9	0.56	0.13±0.03	0.043±0.032	69
8.3	0.60	0.19±0.02	0.038±0.031	77
12.3	0.58	0.17±0.03	0.052±0.036	10
19.7	0.58	0.20±0.03	0.166±0.043	19
32.8	0.66	0.14±0.04	0.107±0.049	38
				52

[a] Defined in Ref. 2.

Normalization and energy calibration of the data dominate the systematic error in $\underline{b}$ (Fig. 8). Uncertainties of 10% (7%) are ascribed to absolute (relative) normalization of data at the two beam energies. The 1% uncertainties is scattered muon energy calibration

at each beam energy are correlated to yield a 1% relative error. The systematic error in b is ±0.032 with only this correlation, rising to ±0.041 with worst-case correlation of 150 GeV energy calibration and normalization. That is, b would lie near zero if, at 150 GeV, scattered energies were raised by 2.6% and cross sections simultaneously were reduced by 18%. However, these shifts would only transform the form of the scale-breaking into a relative depletion of event rate at 150 GeV. Moreover, the χ^2 which measures the overall smoothness and consistency of data at the two energies would rise by more than 40 if these shifts were imposed.

3.3.3 Discussion of results in Method II

The observed scale-noninvariance is insensitive to the assumed form of $\nu W_2(\omega')$, because the data are analyzed within bands of ω. If the Monte-Carlo instead uses a $\nu W_2(\omega')$ which brings the Q^2-averaged ratios in Fig. 7(a)-(h) near unity, b drops by 10%. Other choices of $\nu W_2(\omega')$ produce similar perturbations.[2] The Q^2-dependence of νW_2 for $\omega \lesssim 6$ is coupled to the assumed form of its approach to asymptotic behavior. Use of ω as a scaling variable increases the scale-noninvariance in this range (Fig. 8), while use of $(\omega + 1.4/Q^2)$ largely cancels it. Conversely, the Q^2-dependence of νW_2 for $\omega \gtrsim 6$ is inconsistent with scaling in any variable not wildly different from ω, since νW_2 is nearly independent of ω in this range. Ignoring all data with $Q^2 < 4$ raises the confidence level for scaling in ω' to 14%. Variation of R between ∞ at $Q^2 = 1$ and 0 at $Q^2 = 5$ $(\mathrm{GeV}/c)^2$ can account for only 1/4 of the scale-noninvariance at $\omega \simeq 25$.

4. EXPERIMENTAL SUMMARIES AND CONCLUSIONS

The result of the two tests of scaling are summarized below:

i) From ratio of Fermilab 150-GeV data to 56-GeV data[1]

Scale invariance is tested in ratios of muon scattering cross sections from an iron target at pairs of Q^2 values ranging to 40 $(\mathrm{GeV}/c)^2$ and differing by a factor of 3/8. The apparatus was changed with incident energy to preserve acceptance and resolution in scaled variables. The scale-noninvariant departure from unity of these ratios displays a statistically significant ω-dependence. The effect exceeds the systematic uncertainty by a factor of 1.7.

ii) From comparison of Fermilab 150-GeV and 56-GeV data with SLAC 20-GeV data.[2]

Scale-nonivariance is observed in 150 and 56 GeV muon scattering from an iron target. In the range $1 < Q^2 < 40$ $(\mathrm{GeV}/c)^2$, νW_2 rises with Q^2 at fixed $\omega' \lesssim 6$. The scale-breaking is statistically and systematically significant, and persists with alternate choices of scaling variable. It can be parameterized roughly by a constant $b = \partial^2 \ln(\nu W_2)/\partial \ln(Q^2)$ with a value near 0.09.

Figure 9 shows a crude behavior of νW_2 at large Q^2.

5. POSSIBLE INTERPRETATIONS OF OBSERVED SCALE-NONINVARIANCE

It is too early to tell how to account for the observed effects. We can now offer several rather clear-cut choices and perhaps reject a few obvious ones. No attempts

are made here to be exhaustive or comprehensive. Undoubtedly, new and better approaches to explaining our data are expected.

5.1 Finite parton size[10)]

This obvious choice is not favored here. The rise in Q^2 at large ω cannot be accommodated in this model. Also the constancy of $\langle \underline{r}(Q^2, \omega) \rangle_{Q^2,\omega}$ is not explained. The rise with Q^2 at large ω and fall at small ω is evidence against a form factor $1/(1+\frac{Q^2}{\Lambda^2})^2$. However, if the rise at large ω is a separate phenomenon, the model may still be interesting.

5.2 Charm, color, or new hadronic degrees of freedom

The rise at high ω could be due to a turn-on phenomenon coupled to a clairvoyant choice of scaling variable, say $\omega'' = \omega + 1.4/Q^2$, to account for the low ω behavior. If one were to account for the entire trend of data in one form one must explain a simultaneous rise in Q^2 at large ω and fall in Q^2 at low ω. The observed resonant states J or ψ (3105),[11, 12, 13)] and ψ' (3705)[14)] suggest strongly the existence of a new hadronic degree of freedom such as charm[15)] or color.[16, 17)]

For charm, the new degree of freedom is "hidden"; for color it is "manifest". Can these models lead to an explanation of our effect at large ω?

5.2.1 Charm

The $c\bar{c}$ (c is the charm-quark and $\bar{c}$ anticharm-quark) content of the nucleon is possibly very small. Thus it may have a small effect on the scaling model predictions for μN deep-inelastic scattering. The $c\bar{c}$-quark pair is expected to be as probable as the $s\bar{s}$, $u\bar{u}$, and $d\bar{d}$ pair in the "infinite sea" of quarks. The low energy ep data suggest that the cont ributions of "infinite sea" is small. Is this compatible with the rise at large ω?

5.2.2 Color

Color is introduced to patch up several defects in the usual quark model:

i) It permits one to have a totally antisymmetric wave function for spin-1/2 quarks as expected for fermions. The uncolored quark model, on the other hand, gives a totally antisymmetric wave function.

ii) It gives a higher value of $\sigma_T(e^+ + e^- \to \text{hadrons})$ than a parton-model prediction.

iii) Correction in the anomally calculation of the π^0-lifetime.

A new SU(3) group is introduced.[16)] The Han-Nambu model assumes that all nine quarks make up ordinary hadrons above the threshold for production of color in deep-inelastic scattering, a new scaling region may exist. The 20%-30% excess at large ω could easily be due to such a threshold phenomenon. The threshold would be around W = 5-6 GeV, i.e., $W \geq m(\psi) + m_N$. From the relation $Q^2 \cdot \omega = W_{th}^2$ (= 25-36 GeV^2), the threshold should be located at $Q^2 = 1$ at $\omega = 32.8$, $Q^2 = 2$ at $\omega = 12.3$, and $Q^2 = 5$ at $\omega = 8.3$. An examination of Fig. 7(a)-(d) indicate that this is a perfectly acceptable possibility.

The color scheme, if correct, could be very exciting. For example, in the Han-Nambu scheme it is expected that all $q\bar{q}$ mesons are in the (8, 1); (1, 8), and (8, 8) multiplets of SU(3) × SU(3)'. Baryons are in the usual (10, 1), (8, 1), and (1, 1) colorless

multiplets as well as in $(10, 8)$, $(10, \overline{10})$, $(8, 8)$, $(8, \overline{10})$, $(1, 8)$, and $(1, \overline{10})$. These baryon excited states may eventually show up in electro (muo)-production.

These excited states could possibly appear as narrow missing-mass peaks in $\mu p \rightarrow \mu' +$ missing mass. This potentially very rich situation is one of the main features the follow-on experiment should study in detail. $[M^2 \simeq 2m\nu = 300\ \mathrm{GeV}^2]$.

5.2.3 Strong "new duality"

Another approach suggests that the ψ (3.1) and ψ'(3.7) are colored ω and ϕ mesons, respectively.[18] A prediction is made with "strong new duality" the recurrences of a mass spectra $m_n^2 = m_{\psi,\psi'}^2 + (\Delta m_v^2) \cdot n$, where $n = 0, 1, 2 \cdots$. In this scheme, 72 additional states are expected! How interesting!

5.3 Field theories

One interesting question is whether or not the new Fermilab data provides a clue to the behavior of the moment integrals

$$M_n(Q^2) = \int_1^\infty \frac{\nu W_2(\omega, Q^2)}{\omega^{n+2}}\, d\omega \tag{9}$$

at a large range of kinematic variables.

Two possibilities suggest themselves:

5.3.1 Anamolous moments or dimension[19]

In this case we have a simple power-law dependence:

$$M_n(Q^2) \rightarrow Cn\left(\frac{\mu^2}{Q^2}\right)^{d_n} \text{ as } Q^2 \rightarrow \infty \tag{10}$$

where d_n, if nonzero, define the anamolous dimension. Limiting behavior of this kind is common to conventional field theories in ladder approximation. It is of interest to whether the zeroth-moment behaves as

$$M_o(Q^2) = \int_1^\infty \frac{d\omega}{Q^2}\, \nu W_2(\omega, Q^2) \xrightarrow[Q^2 \rightarrow \infty]{} \text{constant.} \tag{11}$$

The area under the structure function νW_2 should be constant at sufficiently high Q^2 as a result of conserving the stress-energy tensor. In any event, it is possible to describe the muon data with $d_n \simeq 0.2$.

Bjorken scaling requires $d_n = 0$ for all values of n. The data do not favor this conjecture in the kinematic range of $1 \leq Q^2 \leq 50\ (\mathrm{GeV}/c)^2$ and $2 < \omega < 30$. The kinematical bounds on Q^2 and ω is governed by $Q^2 \cdot \omega \leq 260$.

The statistical probablility that data can be fit to a constant for all values of Q^2 and ω in the above mentioned kinematical range is 2×10^{-5}.

5.3.2 Asymptotically free nonabelian gauge field theories[20)]

These theories make the explicit assumption that the effective coupling constant vanishes logarithmically as $Q^2 \to \infty$. [i.e., $d_n = O(Q^2 \log n)$]. The moments for the structure function behave as

$$M_n(Q^2) \xrightarrow[Q^2 \to \infty]{} C_n \left[\frac{1}{\log\left(\frac{Q^2}{\mu^2}\right)} \right]^{A_n} . \tag{12}$$

To account for the Fermilab data, $A_n \approx 0.25$ ($\mu^2 \approx 1$ GeV^2) would be required. The value of A_n in these theories is a measure of the rate at which quarks approach to unbound states.

5.4 Two-photon exchange effects

It is conceivable that at high Q^2 a two-photon exchange diagram may become important.[21)] To test this possibility we have undertaken an experimental study of the ratio of μ^+ and μ^- yields under identical experimental conditions. A preliminary look of the μ^+/μ^- ratio vs Q^2 is shown in Fig. 10 up to $Q^2 = 50$ (GeV/c)^2.

A preliminary analysis places the magnitude of the two-photon amplitude to be less than 2% of the one-photon amplitude. Further analysis is still in progress.

5.5 Shadowing,[22)] μ-e universality,[23)] radiative effects,[24)] and others

Although further analyses are needed to place upper limits of these effects in the data, there is no reason to expect anomalous behavior here. More detailed discussion of these will be given elsewhere.

6. NEW ISSUES (1975) IN DEEP INELASTIC PHENOMENA

The observed deviation from scale-invariance suggests that instead of adopting a simplified picture in the structure of nucleons, we now need an appraisal. Fig. 11 shows a current outlook in deep-inelastic continuum.

New issues are being raised. We cite a few examples:

i) Does the set of new data imply a new scale? If so, what is the magnitude of the scale (i.e., the characteristic mass)?

ii) Is the nonscaling observed only in νW_2? Does W_1 scale? Since the μ experiment measures events at extremely small laboratory angles, it is not sensitive to the values of W_1. SLAC could possibly study the Q^2-dependence in W_1 at moderate Q^2 [< 30(GeV/c)^2].

iii) What is the functional form of $R(Q^2, \omega)$?

iv) If the rise in Q^2 at large ω were due to some new hadronic degrees of freedom, should there be an observable step in νW_2? Are there new particles in deep inelastic collisions?

v) How does one now approach the study of hadron final states in deep inelastic scattering?

vi. If the nonscaling is associated with charm, color of other schemes, can one detect new excited states (as missing mass peaks) in muo-production?

vii. Is the observed pattern of nonscaling due to a combination of two or more scaling-breaking effects? If so, how can one distinguish them?

viii. Is there a way to reconcile the observed pattern in e^+e^- annihilation and deep-inelastic scattering?

Some of these questions can be answered with more precise data and data at high Q^2 and ω. A higher intensity muon beam now exists at Fermilab. At CERN SPS a high intensity muon beam is planned for 1977.[25] New data in a larger kinematical range (Fig. 12) should be available shortly both from a new round of muon scattering experiments at Fermilab[26] and at CERN.

7. CONCLUSION

During the past year our views on scaling in deep-inelastic scattering is beginning to change. We now entertain the idea that as one reaches sufficiently high Q^2 and W^2, strict Bjorken scaling may not be valid. In particular in the large ω region, the observed rates exceed the scaling predictions (using SLAC structure function at low energy) by as much as 20-30%. At low values of ω' there is evidence for a depletion of events when the scaling variable ω' is used. The nonscaling at low ω' can in principle be patched up by selecting a new kind of scaling variable such as $\omega'' = \omega + 1.4/Q^2$. A continual change of scaling variable would, on the other hand, render the concept of scale-invariance somewhat less appealing.

When viewed together with discoveries of narrow resonant states $\psi(3100)$ and ψ' (3705), the large ω effect might support the existence of some new hadronic degrees of freedom such as charm, color, or other exotic schemes. On the other hand, a logarithmic behavior for the moments of structure functions at high Q^2 cannot be ruled out at this time.

More important tests are yet to come. Detailed study of missing mass spectra, search of directly produced objects (short-lived particles), further measurements of structure function at higher Q^2 and W^2 are important milestones.

Overall we are now entering a critical stage in our understanding the role of quarks as fundamental entities in hadron physics. We might be closer now to find a picture of hadronic interactions, based on a field theory with fundamental fermion fields carrying quark quantum numbers. We might soon be able to unify our understanding on hadron spectroscopy, deep-inelastic scattering, and e^+e^- annihilation.

Note added in proof: At this conference, R. Taylor (SLAC) presented some evidence for scaling-breaking in W_1 up to $Q^2 \simeq 30\ (\mathrm{GeV}/c)^2$.[27] It is evident that a depletion of the order of -20% is seen in W_1. Since the muon results concern itself with νW_2, the connection between the Fermilab and SLAC results is not readily obvious.

REFERENCES

1. Y. Watanabe et al., paper submitted to this conference.
2. C. Chang et al., paper submitted to this conference.
3. J. D. Bjorken, Phys. Rev. 179, 1547 (1969).
4. W. K. H. Panofsky, Proceedings of VIVth International Conference on High Energy Physics, Vienna, Austria, 1968, p. 23.
5. E. D. Bloom et al., Phys. Rev. Lett. 23, 930 (1969); M. Breidenbach et al., Phys. Rev. Lett. 23, 935 (1969).
6. For a review, see F. J. Gilman, in Proceedings of the XVII International Conference on High Energy Physics, London, England, 1974, edited by J. R. Smith, p. IV-149.
7. E. D. Bloom and F. J. Gilman, Phys. Rev. D4, 2901 (1971); E. M. Riordan et al., Phys. Rev. Lett. 52B, 249 (1974).
8. D. J. Fox et al., Phys. Rev. Lett. 33, 1504 (1974).
9. M. Chanowitz and S. Drell, Phys. Rev. Lett. 30, 807 (1973).
10. J. S. Poucher et al., Phys. Rev. Lett. 32, 118 (1974).
11. J. J. Aubert et al., Phys. Rev. Lett. 33, 1404 (1974).
12. J.-E. Augustin et al., Phys. Rev. Lett. 33, 1406 (1974).
13. C. Bacci et al., Phys. Rev. Lett. 33, 1408 (1974); Erratum, Phys. Rev. Lett. 33, 1649 (1974).
14. G. S. Abrams et al., Phys. Rev. Lett. 33, 1453 (1974).
15. The case for charm has been particularly argued for by T. Appelquist and H. D. Politzer, Phys. Rev. Lett. 34, 43 (1975); A. De Rujula and S. L. Glashow, Phys. Rev. Lett. 34, 46 (1975); T. Appelquist et al., Harvard preprint, 1974 (unpublished); and by M. K. Gaillard, B. W. Lee, and J. L. Rosner, FNAL preprint Pub-74/86-THY.
16. M. Y. Han and Y. Nambu, Phys. Rev. 139B, 1006 (1965).
17. J. C. Pati and A. Salam, Phys. Rev. Lett. 32, 1083 (1974).
18. D. Schildknecht and F. Steiner, Phys. Lett. 56B, 36 (1975); M. Kramer, D. Schildknecht and F. Steiner, DESY 74/64 (1974).
19. K. G. Wilson, Phys. Rev. 179, 1499 (1969).
20. D. Gross, Phys. Rev. Lett. 32, 1071 (1974).
21. P. Fishbane and Kingsley, Phys. Rev. D8, 3074 (1973).
22. N. Nikolaev and V. Zakharov, Phys. Lett. 55B, 397 (1975).
23. BNL, SLAC μ experiments.
24. R. H. Siemann et al., Phys. Rev. Lett. 22, 421 (1969).
25. E. Gabathuler and F. Brasse (private communication).
26. Experiment 319, Fermi National Accelerator Laboratory; other muon scattering experiments are also planned. (E-98)
27. R. Taylor, invited paper presented at this conference.

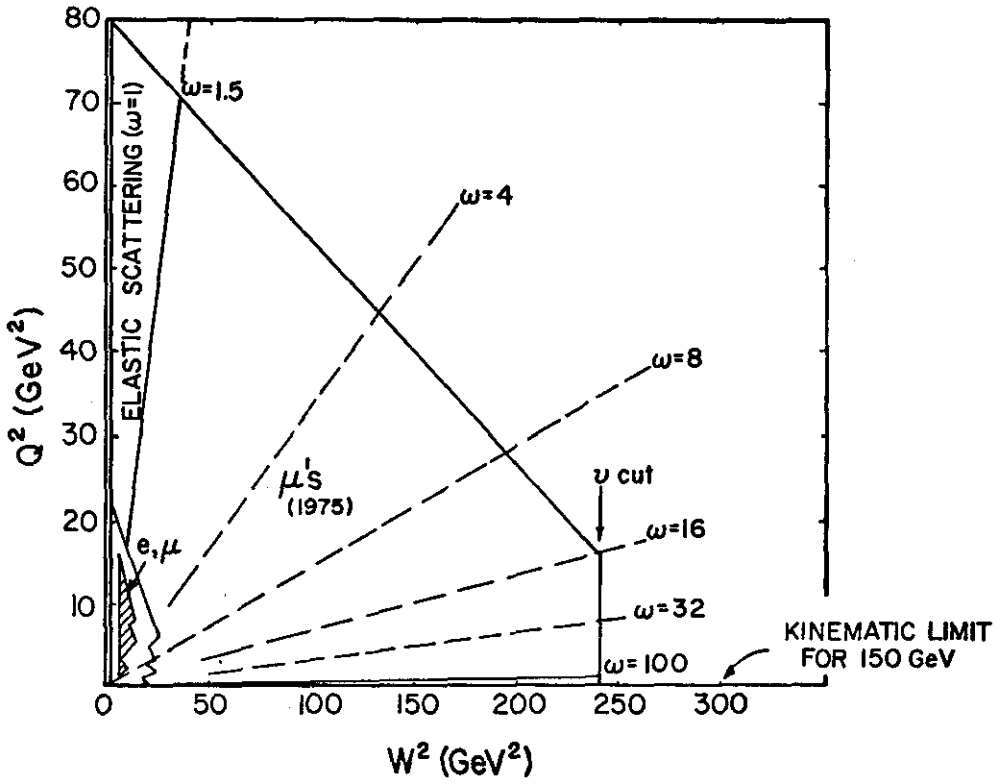

Fig. 1. Kinematic range of Q^2 and ω reached in the muon deep-inelastic scattering experiment at 150 GeV and 56 GeV.[1,2] (1975)

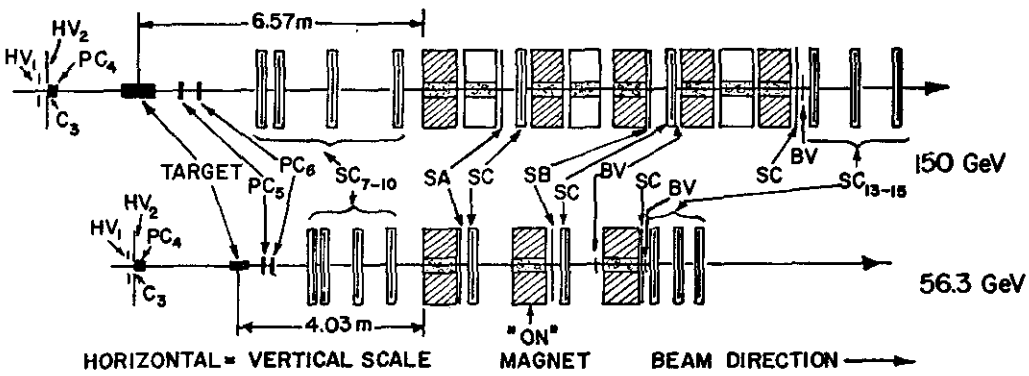

Fig. 2. Apparatus for muon scattering experiment at Fermilab.

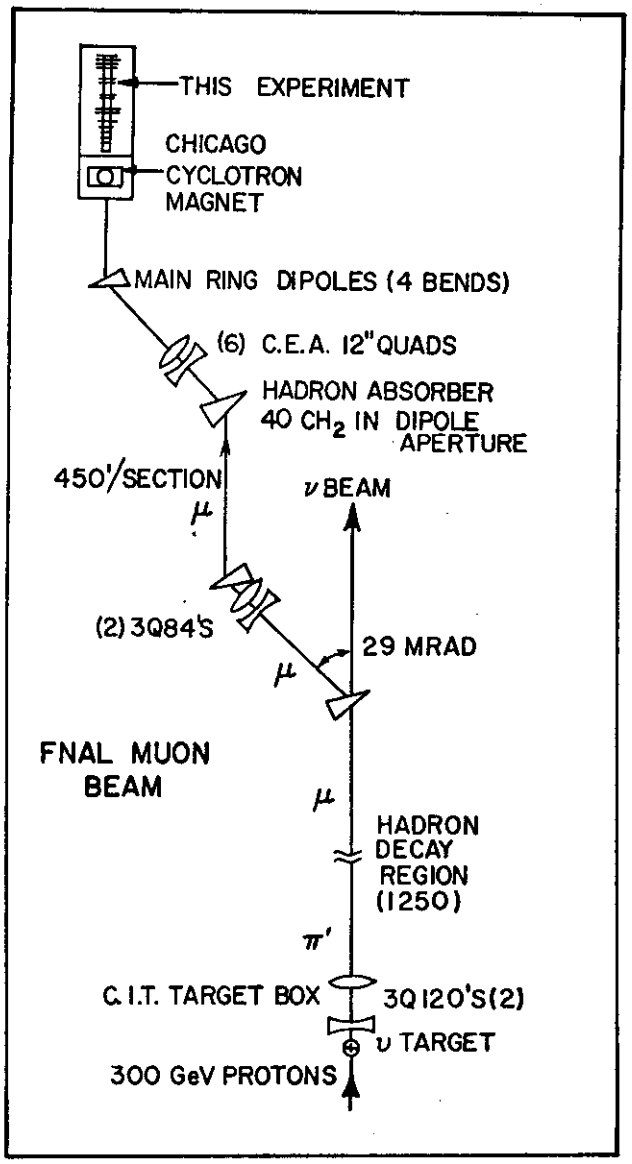

Fig. 3. Fermilab muon beam layout.

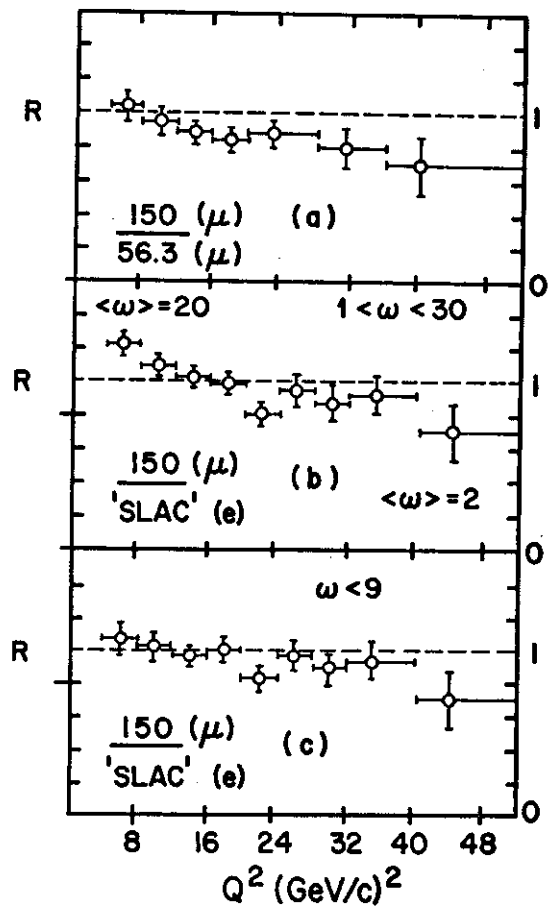

Fig. 4. Early tests of scaling in muon scattering. (1974). Note that in b) the "rise" in at $\langle Q^2 \rangle = 8\ (\mathrm{GeV}/c)^2$ [$\langle \omega \rangle = 20$] is already in evidence. A slight "fall" is also visible at $\langle Q^2 \rangle = 44\ (\mathrm{GeV}/c)^2$ [$\langle \omega \rangle = 2$].

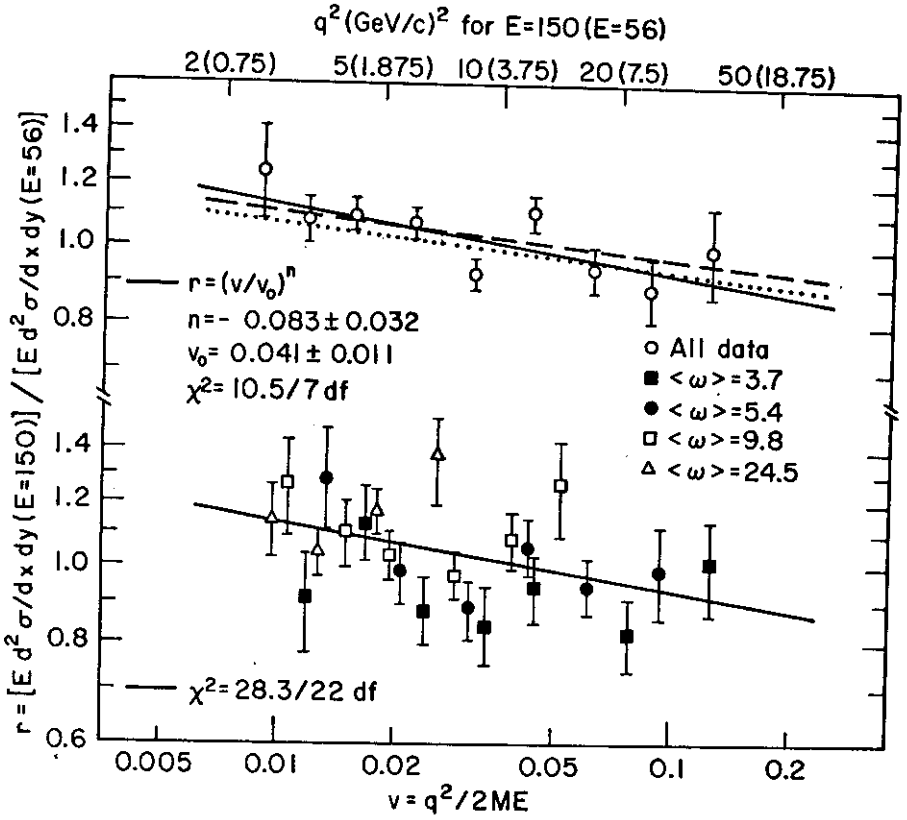

Fig. 5. $\underline{r}(Q^2, \omega)$ plotted vs $v(=Q^2/2ME)$ only. (1975)

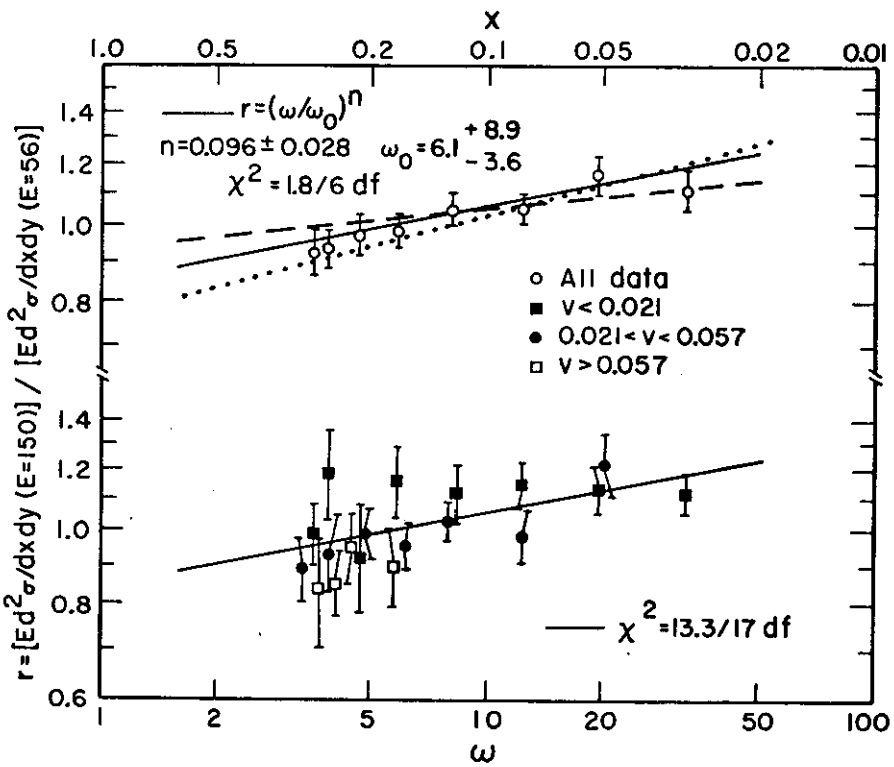

Fig. 6. $\underline{r}(Q^2, \omega)$ plotted vs ω only. (1975)

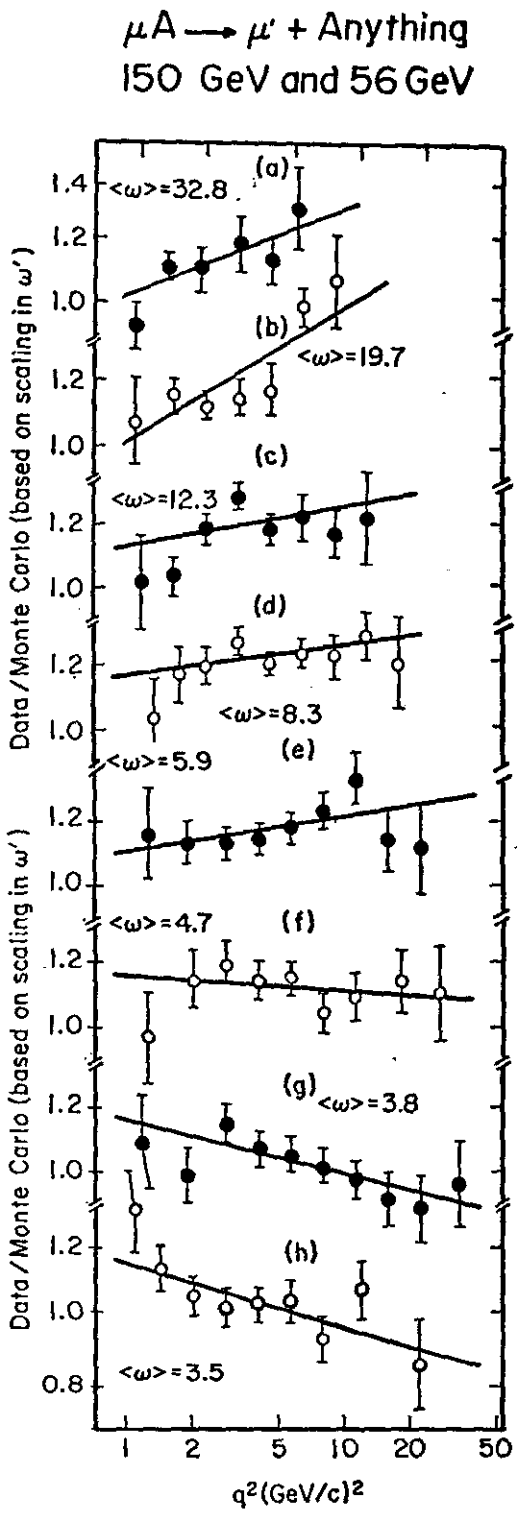

Fig. 7. Ratio of observed to Monte-Carlo rate vs Q^2 for 8 ranges of ω. Widths of these ranges and parameters of the straight-line fits are detailed in Table 2. Errors are statistical. (1975)

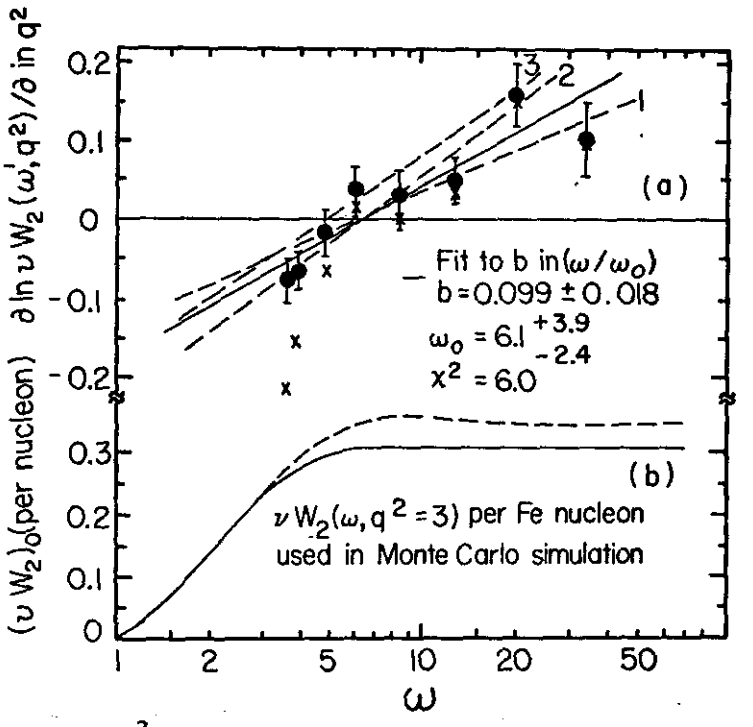

Fig. 8. (a) slopes in $\ln(Q^2)$ for the 8 ω ranges. Errors are statistical. Dashed lines depict effects of (1) raising E' by 1% at 150 GeV, (2) same at 56 GeV, (3) raising 150 GeV cross sections by 7%. Assuming scaling in ω rather than ω' in the Monte-Carlo yields the points indicated by "X".

(b) $\nu W_2(\omega, Q^2=3)$ per nucleon used in the Monte Carlo, with scaling in ω' and R=0.18. The dashed line is the alternate form described in the text.

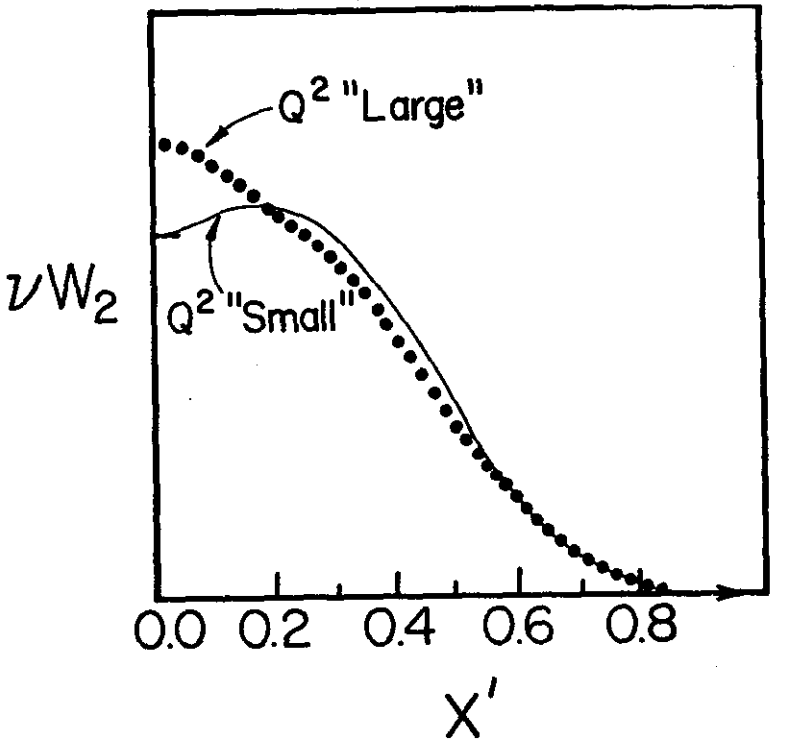

Fig. 9. Crude behavior of $\nu W_2(\omega')$ at high Q^2.

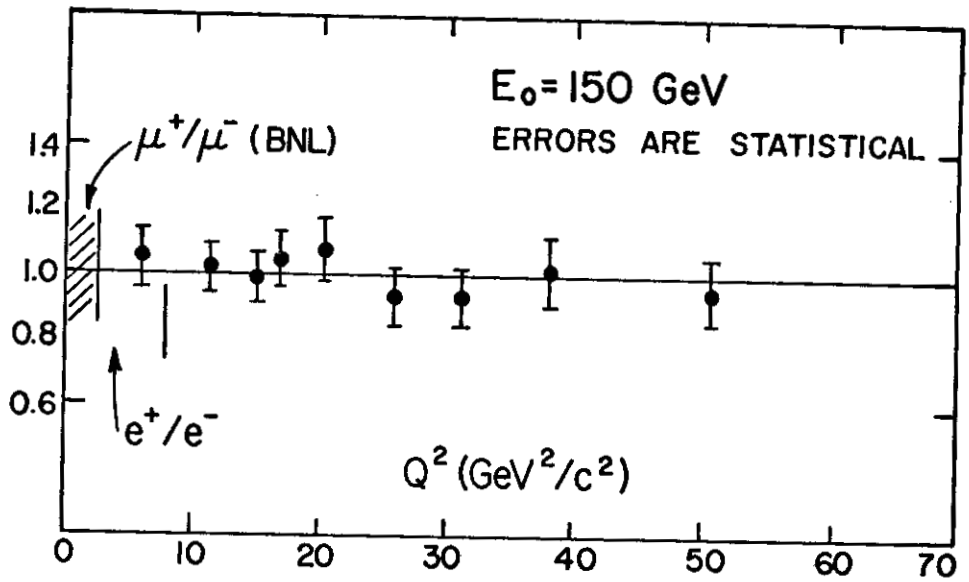

Fig. 10. Preliminary data on μ^+/μ^- ratio at 150 GeV vs Q^2.

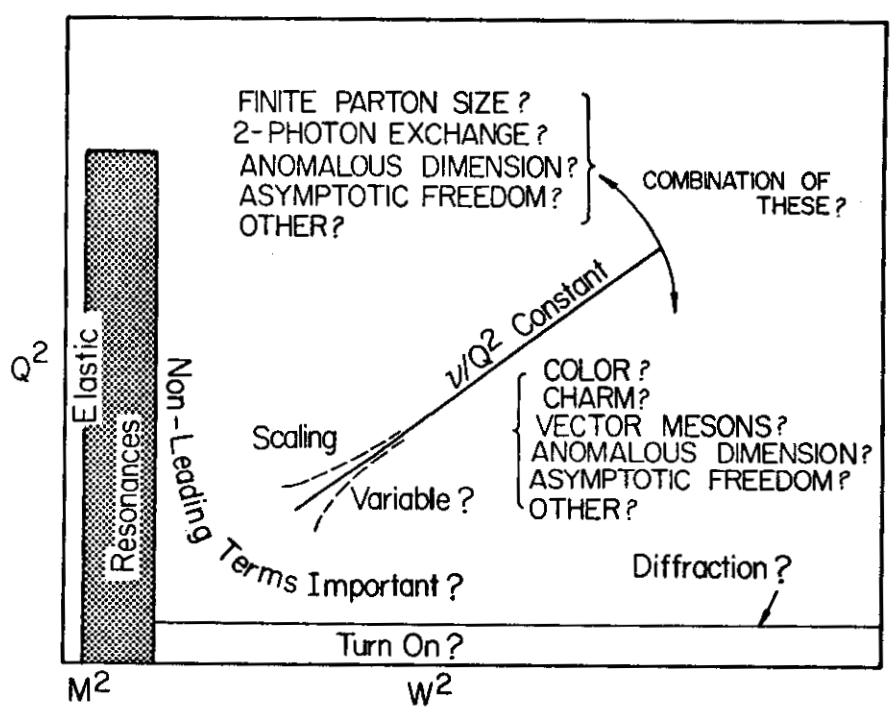

Fig. 11. Current outlook for deep inelastic scattering.

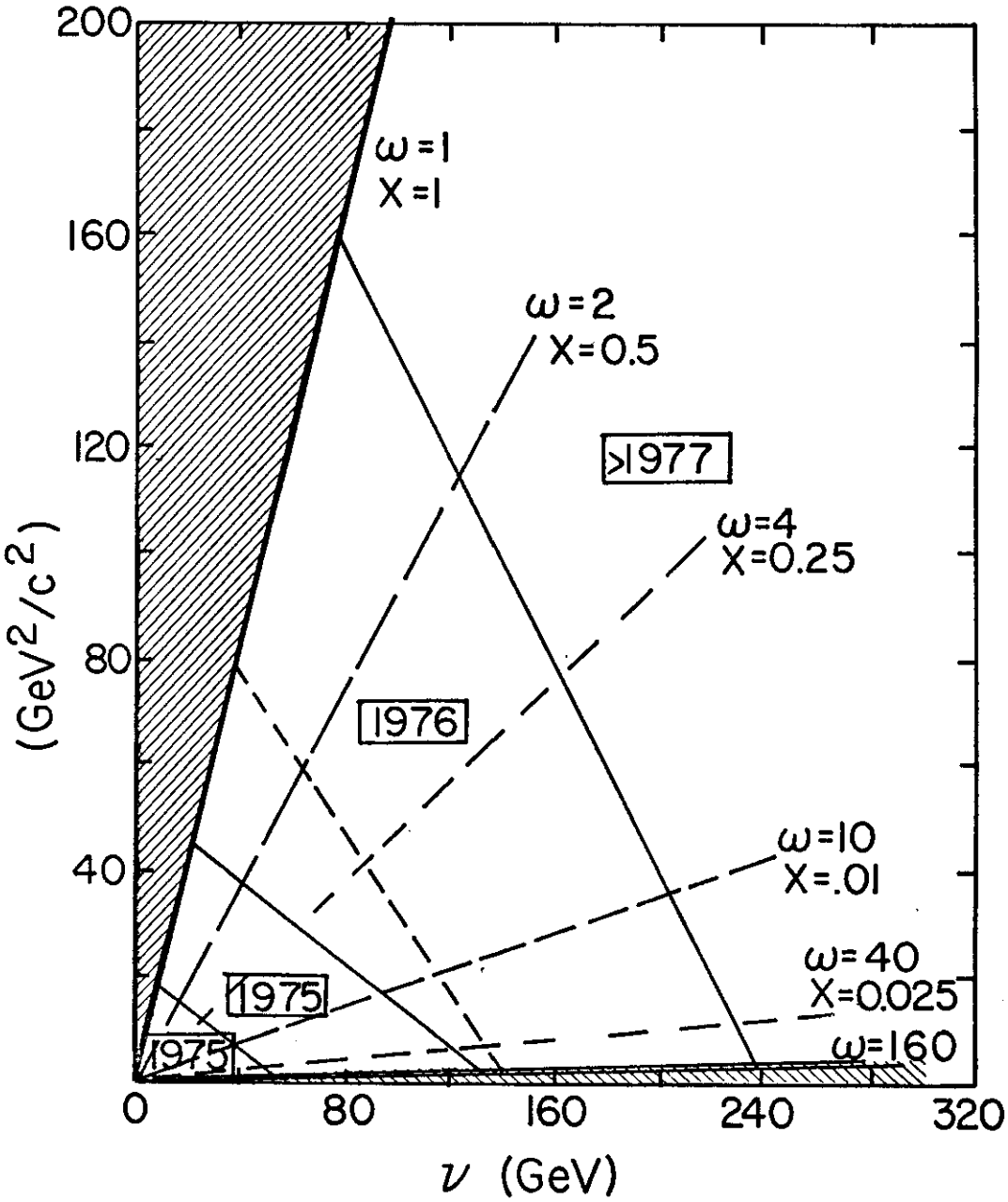

Fig. 12. Kinematic range of data for the next round of μ-scattering experiments (>1976).